Chapter 6

DEVELOPMENT AND APPLICATION OF A PROCESS WINDOW FOR ACHIEVING HIGH QUALITY COATING IN A FLUIDIZED BED COATING PROCESS

Abstract

Next to the coating formulation, process conditions play important roles in determining coating quality. This study aims to develop an operational window that separate layering from agglomeration regimes and furthermore the one that leads to the best coating quality in a fluidized bed coater. The bed relative humidity and the droplet size of the coating aerosol were predicted using a set of engineering models. The coating quality was characterized using a quantitative image analysis method, which measures the coating thickness distribution, the total porosity and the pore size distribution in the coating. The layering regime can be achieved by performing the coating process at a certain excess of the viscous Stokes number (ΔSt_v). This excess is dependent on the given bed relative humidity and droplet size. The higher the bed relative humidity, the higher is the ΔSt_v required to keep the process in the layering regime. Further, it is shown that using bed relative humidity and droplet size alone is not enough to obtain constant coating quality. The changes in bed relative humidity and droplet size have been identified to correlate to the fractional area of particles sprayed per unit of time. This parameter can effectively serve as an additional parameter to be considered for a better control on the coating quality. High coating quality is shown to be achieved by performing the process close to saturation and spraying droplets small enough to obtain high spraying rate but not too small to cause incomplete coverage of the core particles.

Published in AAPS PharmSciTech 10(3): 732-742 (2009)

6.1. Introduction

Fluidized bed coating technology is frequently applied in the production of micro-encapsulated products, which are of interest of many industries, such as the pharmaceutical industry. It offers the possibility to alter and to improve various characteristics of core particles such as the surface properties in a single unit operation. The challenges of using this technology are the difficulties in choosing the proper process conditions that lead to a constant coating quality and a robust process, especially during process up-scaling. One of the typical problems encountered is the occurrence of excessive core agglomeration that leads to process failure. Another problem is the occurrence of spray-drying of the coating aerosol, which should also be avoided although it is less harmful for the continuity of process. Both cases result in poor coating quality (46, 65). Therefore, it is desirable to perform coating within the layering or in the coating regime (46).

Understanding of the impact of process settings on the particle growth regimes has been the subject of many investigations, while less works focused on their impact on coating structures. Considering the importance of both aspects on product development, this work investigates the process settings that separate layering from agglomeration regimes and from that it defines the process regime that leads to the best coating quality.

Iveson and Litster (150) proposed the distinction of various particle growth regimes inside drum granulation using the Stokes deformation number and the maximum pore saturation. The application of this regime map for fluidized bed coating process is however not straightforward. The prediction of the granule growth regime requires information on the granule properties *i.e.* granule density, yield stress and porosity, which are not known before the process is performed. Moreover, the fluidized bed coating process involves different parameters from a mechanically agitated granulation process, which makes this regime map can not readily be applied for the fluidized bed coating process.

In a fluidized bed process where the shear force on particles is quite low, the agglomeration tendency is rather governed by the particle coalescence than by the breakage of the granules. The successfulness of the particle coalescence depends on the availability of the liquid at the particle surface and the strength of the liquid bridge between two particles to facilitate a successful coalescence (151). To avoid particle coalescence or in other words to have a situation where colliding particles rebound, the kinetic energy upon particle collision has to exceed the viscous dissipation in the liquid and elastic losses in the solid phase (152). Ennis *et al.* (153) proposed that to be in the layering regime the viscous Stokes number (St_v)

has to be much higher than less than the critical viscous Stokes number (St_v^*), defined in Eqs. 6-1 and 6-2 (152), respectively.

$$St_v = \frac{2\rho_p d_p u_p}{9\mu} \tag{6-1}$$

$$St_v^* = \left(1+\frac{1}{e}\right)\ln\left(\frac{h}{h_a}\right) \tag{6-2}$$

This model was developed by assuming elastic collisions between non-deformable particles. In practice, the particles can become deformable upon wetting by the coating liquid. The bed relative humidity and the droplet size are key parameters determining the availability of the wetting liquid on the particle surface (154-156), which then can influence the collision behavior between (wet) particles. This becomes the rationale in this study to take into account these factors together with the excess Stokes criteria in the prediction of coating regime inside the fluidized bed coater.

The bed relative humidity was predicted using mass and heat balance equations (157-158), in which the non-adiabatic situation in the coating process was considered extending the common adiabatic assumption in practice. The correlation between these process conditions and the coating quality was developed using the coating characterization results, which were obtained by performing quantitative image analysis on the images of coated particles.

6.2. Theory

6.2.1. Particle Coalescence inside a Fluidized Bed Coater

In a fluidized bed, particle velocity varies according to the variations in the particle size and particle position, leading to a variation in the Stokes number at a certain process condition. This explains the difficulty in determining the excess of Stokes number (St_v - St_v^*) required to be in the coating regime. In this study, we attempted to estimate this criterion.

Eqs. 6-1 and 6-2 were used to calculate St_v and St_v^*, where ρ_p, μ, d_p, u_p, e, h, h_a are the particle density, the viscosity of the coating solution, the (harmonic) mean diameter of two particles, the impact velocity, the coefficient of restitution, the thickness of the liquid layer at particle surface, and the characteristic height of surface asperities, respectively. The St_v was calculated using the maximum particle velocity and the median particle size, while the St_v^* was calculated using the maximum droplet height. In this way, the occurrence of

agglomeration can be predicted, which occurs when the excess of Stokes number is below the suggested limit.

In this study, the u_p was taken to be the maximum particle velocity. The h was taken to be the height of the droplet, which was calculated assuming a spherical cap droplet on a flat and smooth surface. It is realized that the core particles used in the fluidized bed coating process were not flat and smooth. However, the size of the spayed droplets was relatively small in comparison to the particle size used. Therefore, the curvature of the core particles can be assumed negligible. The h_a was calculated as the half of the difference of the maximum and the mean diameter of the granule. It is a measure of the surface roughness of the core particles. The data properties used in the calculation are presented in Table 6-1. Relative to the particle sizes used, h_a is very small, therefore, the assumptions used during the calculation of droplet height are considered acceptable.

Table 6-1. Properties of materials used in this study.

Materials	**Diameter (μm)**	**Density (kg/m^3)**	**h_a (μm)**
Microcrystalline Cellulose	275	1463	8.5
	755	1463	31.1
	900	1463	32.0
Ethisphere®	275	1518	31.9
Sanal® P	512.5	2493	7.2
Glass beads	460	2493	3.7
	1000	2531	2.9
	4000	2517	1.9
Suglets®	1550	1581	14.1
EVA	3714	929.6	1.9
	Density (kg/m^3)	**Viscosity (Pa.s)**	**Surface tension (N/m)**
HPMC E5	1328	-	-
HPMC E5 solution (159)	271.6224Xp + 996.459	3.173exp(42.145Xp)/1000	-3.9286Xp^2+0.425Xp + 0.45057

6.2.2. Mass and Heat Exchange in Fluidized Bed Coating Process

Fluidized bed coating process is a multiphase process, where the coating layer is ideally built gradually in time. The sprayed polymer droplets hit the particles and are dried as a result of which they are deposited on the core substrate and form a coating layer (160). Schematically, it can be depicted as in Figure 6-1.

This chapter focuses on the application of an aqueous coating solution. Therefore, the mass and the heat exchange during the process involves mainly the air and water components having certain conditions at the inlet (subscript *in*) and the outlet (subscript *out*) as represented in Figure 6-1 (bottom). In this case, the water term also includes the moisture contained in air and the water contained in coating solution. The control volume was taken to be the volume between the air distributor and the top of the fluidized bed column. The symbols used in this paper can be found in the list of symbols.

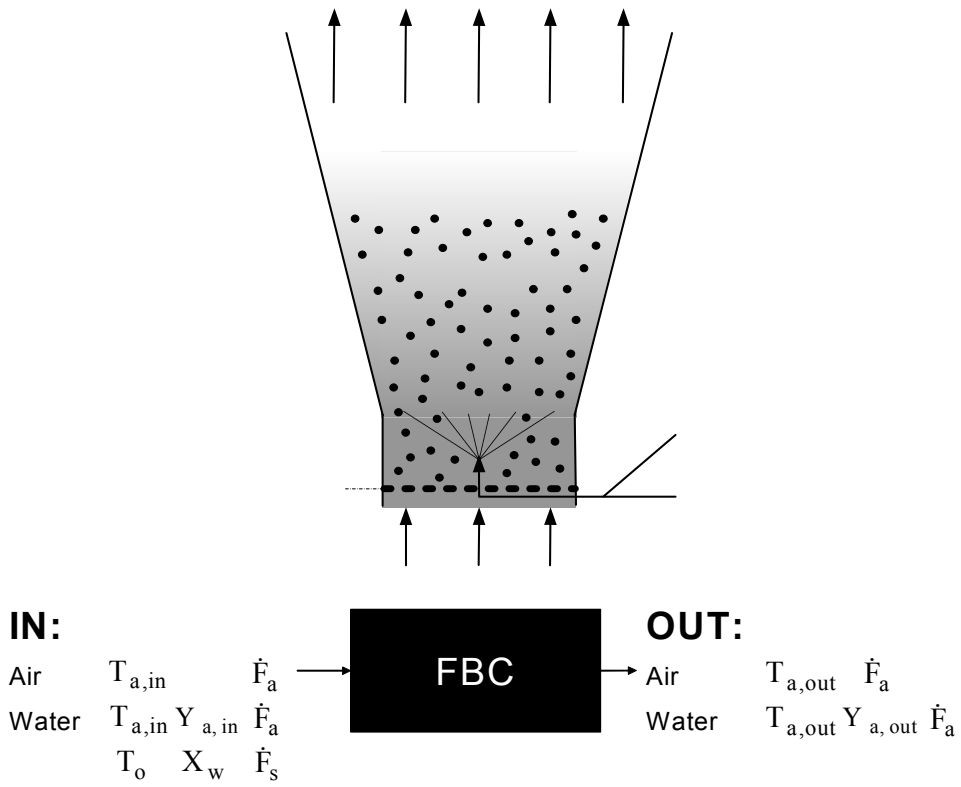

Figure 6-1. Schematic representation of fluidized bed coating process

The heat transfer in fluidized bed is known to be highly efficient. Therefore, the evaporation of water by hot air is assumed to occur instantaneously. Here, the system is assumed to be in the steady state condition, implying that the amount of water sprayed is equal to the amount of water leaving the system, as given in Eq. 6-3. Based on this equation, Eq. 6-4 can be derived.

$$\dot{F}_{water,in} = \dot{F}_{water,out} \tag{6-3}$$

$$Y_{a,in} \cdot \dot{F}_a + X_w \cdot \dot{F}_s = Y_{a,out} \cdot \dot{F}_a \tag{6-4}$$

This assumption is of course not true when the amount of water sprayed exceeds the drying force of the introduced air. However, this assumption was used considering that it

enables the inclusion of the over-wetting effect during the heat balance calculation, which therefore results in a correct calculation of the bed relative humidity.

The total enthalpy supplied into the fluidized bed coating system is the sum of the enthalpy of air in the inlet air, the enthalpy of moisture in the inlet air and the enthalpy of the sprayed water, as depicted in Eq. 6-5. The total enthalpy leaving the system is the sum of the enthalpy of the air in the outlet air, the enthalpy of moisture in the outlet air and the heat loss to the surroundings, as given in Eq. 6-6. Here, room temperature (T_o) was used as temperature of reference. λ, Cp_a, and Cv_w represent specific heat of evaporation, specific heat capacity of air and water vapor, respectively.

$$\dot{Q}_{total,in} = Cp_a \dot{F}_a \left(T_{a,in} - T_o\right) + Cv_w Y_{a,in} \dot{F}_a \left(T_{a,in} - T_o\right) \tag{6-5}$$

$$\dot{Q}_{total,out} = Cp_a \dot{F}_a \left(T_{a,out} - T_o\right) + Cv_w Y_{a,out} \dot{F}_a \left(T_{a,out} - T_o\right) + X_w \dot{F}_s \lambda + heat\ loss \tag{6-6}$$

Based on the steady state assumption, the total enthalpy going out of the system is equal to the total enthalpy coming into the system. The fluidized bed system is often not fully insulated, resulting in a certain heat loss. The heat loss is dependent on the difference between the process temperature and the temperature of its surroundings. It is characterized by the heat loss coefficient ($C_{heatloss}$), that is normally dependent on several variables *e.g.* equipment dimensions and material (125). Using these assumptions, the heat loss in Eq. 6-6 could be substituted with the term $C_{heatloss}\left(T_{a,out} - T_o\right)$. Thereby, Eqs. 6-3 to 6-6 were solved deriving an equation (Eq. 6-7) which calculates the temperature of air at the outlet.

$$T_{a,out} = T_o + \frac{\left(Cp_a + Y_{a,in} Cv_w\right)\dot{F}_a \left(T_{a,in} - T_o\right) - X_w \dot{F}_s \lambda}{Cv_w \left(X_w \dot{F}_s + Y_{a,in} \dot{F}_a\right) + Cp_a \dot{F}_a + C_{heatloss}} \tag{6-7}$$

6.3. Material and Methods

6.3.1. Materials

Various pellets were used as cores comprising of:

(i) Microcrystalline cellulose pellets (250-300 μm, 710-800 μm, 800-1000 μm), which were made from Avicel PH102 (FMC BioPolymer, Philadelphia, USA) using method described in Laksmana *et al.* (161);

(ii) Ethispheres® (300-350 μm), which are manufactured microcrystalline cellulose pellets, a gift from NP Pharm (Bazainville, France);

(iii) Sodium chloride particles, Sanal® P (425-600 μm), a gift from Akzo Nobel Salt (Amersfoort, the Netherlands);

(iv) Glass beads (400-520 μm, 1000 μm and 4000 μm), and

(v) EVA pellets (ATEVA® 1075A, AT Plastics Inc., Alberta, Canada), which are ethylene vinyl acetate copolymer resins containing 9% vinyl acetate. The pellets were hand-sieved in order to obtain a specific particle size range.

Hydroxypropyl methylcellulose/HPMC (Methocel E5 LV USP/ EP premium grade, Dow) supplied by Colorcon (Dartford Kent, UK) was used as the coating material. Carmoisine (E122, Pomona BV, Hedel, the Netherlands) was used as the pigment in the coating. HPMC solution was made by dissolving HPMC polymer and carmoisine in cold water and stirring it for at least 1 hour to assure the homogeneous solution.

6.3.2. Experimental Methods

6.3.2.1. Fluidized Bed Coating Process

The pellets were coated in a fluidized bed coater (Mycrolab, Oystar Hüttlin, Schopfheim, Germany). The HPMC solution was sprayed either from the bottom or from the top of the column. The coating process was performed until about 20% ratio of coating to core weight was sprayed. Various coating processes with different types and amounts of particle cores, different HPMC concentrations and different process conditions were performed, which are listed in Table 6-2.

6.3.2.2. Determination of Droplet Size

The droplet size was determined using the simplified model from Nukiyama and Tanasawa (162), which have been commonly used in practice (Eq. 6-8) (159).

$$d_d = \left[\frac{585000}{u_{a,tip} - u_{s,tip}}\right] \times \left[\frac{\gamma}{\rho_s}\right]^{0.5} + 1683\mu^{0.45}\left[\gamma \times \rho_s\right]^{-0.225}\left[\frac{1000}{Q_{a,orifice}/Q_{s,tip}}\right]^{1.5} \quad (6\text{-}8)$$

Pre-calculation steps were performed to calculate the $u_{a,tip}$, $u_{s,tip}$, $Q_{a,orifice}$, and $Q_{s,tip}$ using Eqs. 6-9 to 6-13, respectively (125). In these equations, k (the ratio between Cp and Cv) was taken to be 1.4 for air, while the dimensions of the nozzle: d_n and $d_{orifice}$ were 0.6 and 1.2 mm, respectively. The HPMC solution properties used for the calculation are given in Table 6-1.

Table 6-2. Experimental program used in this study (MCC-Microcrystalline cellulose pellets; ES-Ethispheres®; GB-glass beads; EVA- ethylene vinyl acetate copolymer (9% vinyl acetate) resins).

No.	Core type	Spraying direction	Bed mass (g)	X_{HPMC}	Q_{fa} (m^3/h)	P_{atm} (bar)	$\dot{F}_s$ (g/min)	$T_{a,in}$ (K)	$T_{a,out}$ (K)
1	MCC 800-1000µm	BS	150	5%	25	1.5	6.6	343.2	301.7
2						1.5	5.0	343.2	306.8
3						1.5	2.4	343.2	313.8
4						0.5	2.4	343.2	314.1
5						1.5	2.4	333.2	308.7
6						1.5	4.8	323.2	296.4
7						1.5	2.4	323.2	302.8
8						1.5	2.4	313.2	296.7
9						1	2.4	313.2	297.2
10						0.5	2.4	313.2	297.2
11		TS				0.5	4.8	343.2	309.2
12	Salt 425-600µm	BS	150	5%	25	1.5	3.0	333.2	305.0
13					20	1.5	3.0	333.2	301.2
14					20	1.5	3.0	313.2	294.6
15	ES 300-355µm	BS	150	5%	25	1.5	3.6	343.2	312.2
16	GB 400-520µm	BS	150	5%	25	1.5	3.0	333.2	307.0
17	GB 4000µm		50			1.5	1.2	333.2	310.5
18						1	1.2	333.2	313.5
19						0.5	1.2	323.2	308.2
20						0.5	1.2	313.2	302.7
21	MCC 800-1000µm	BS	150	5%	15	1.5	2.4	343.2	291.7
22					25	1.5	5.0	353.4	314.1
23						1.5	4.0	353.9	315.7
24						1.5	4.8	313.2	294.3
25						1.5	4.8	343.2	305.4
26						1	4.8	343.2	307.5
27						0.5	4.8	343.2	307.6
28						1	2.4	343.2	313.7
29	MCC 250-300µm					1.5	4.2	333.2	303.2
30	MCC 710-800µm					1	3.0	333.2	307.2
31	MCC 800-1000µm			10%		0.5	4.2	343.1	310.9
32						0.5	3.0	343.1	312.7
33		TS		5%		1.5	4.8	343.1	305.9
34	EVA 3600-3800µm	BS	50	5%	25	1.5	2.8	343.1	313.2
35						1.5	1.4	343.1	315.8
36						1.5	1.4	313.2	300.0
37	GB 4000µm	BS	50	5%	20	1.5	2.4	333.2	310.5
38					25	0.5	1.2	333.1	313.3
39	GB 1000µm	BS	60	5%	25	0.5	5.8	333.2	307.8
40	Suglets 1400-1700µm	BS	50	5%	25	1.5	3.0	343.2	311.9
41						1.5	1.2	343.1	316.2
42						1.5	1.2	343.1	315.3

$$u_{a,tip} = \sqrt{\frac{2kRT_0}{(k+1)Mw_a}} \tag{6-9}$$

$$u_{s,tip} = \frac{\dot{F}_s}{0.25\pi d_n^2 \rho_s} \tag{6-10}$$

$$\rho_{a,cr} = \left(\frac{2}{k+1}\right)^{1/(k-1)} \rho_a(T_0) \tag{6-11}$$

$$Q_{a,orifice} = \frac{P_n A_{orifice} \sqrt{\left(\frac{2}{k+1}\right)^{(k+1)/(k-1)} \left(\frac{kMw_a}{RT_0}\right)}}{\rho_{a,cr}} \tag{6-12}$$

$$Q_{s,tip} = \frac{\dot{F}_s}{\rho_s} \tag{6-13}$$

In this study, the initial droplet size was varied by changing the atomization pressure (between 0.5 to 1.5 bar) and the concentration of the HPMC solution (from 5% to 10%). The droplet sizes obtained vary between 33 to 364 μm.

6.3.2.3. Determination of Particle (Impact) Velocity

The particles inside the fluidized bed equipment were tracked using a high speed camera (Motion Xtra HG-100K, Redlake, Tallahassee, USA). The camera was placed in front of the monitor glass, which is a few centimeters above the air distributor. The images were recorded at speed of 3000 frames per second, which enables the determination of the particle velocity in the range studied. The obtained images are 736x768 pixels in size and have a pixel size of 12.98 μmx13.33 μm.

The particle velocity was determined by tracking the particle displacement over time, which was performed using Motion Pro Studio™ software (IDT Vision, Lommel, Belgium). The particle velocity was determined as the maximum velocity of 15-20 particles, which were tracked for each test performed.

Particle velocities of various particle sizes at different fluidizing air velocities were measured, from which data a correlation for particle velocity was developed. The model used is similar to that of Kunii and Levenspiel (163). Some of the parameters had to be derived empirically, due to the differences in the air distributor and the design of the fluidized bed column used in this study. The obtained correlations are shown in Table 6-3.

Table 6-3. Correlation for the particle velocity (U_p) and its constants as a function of the particle size (d_p), particle density (ρ_p), and inlet air velocity (U_{fa}).

$$U_p = b_1 \rho_p d_p^{-b_2} \left(U_{fa} - b_3 \rho_p d_p^{b_4} \right)^{b_5}$$

Constants	Values
b_1	10.673
b_2	0.279
b_3	2.764×10^{-5}
b_4	1.233
b_5	1.037
R^2	0.974

6.3.2.4. Determination of the Agglomeration Occurrence

The occurrence of agglomeration was monitored by measuring the particle size before and after coating process. The agglomeration was signified when the size of more than 10% weight fraction of the particles is larger than the cut-off diameter. The cut-off diameter was determined by calculating the maximum size of coated pellets obtained after coating process if the coating film was formed by layering. This criterion differs for the core particles used, as listed in Table 6-4.

Table 6-4. Cut-off coated pellets diameter to determine the occurrence of agglomeration in experiments.

Core particles	Cut-off diameter (μm)
MCC 250-300 μm	315
MCC 710-800 μm	830
MCC 800-1000 μm	1040
ES 300-350 μm	365
Salt 425-600 μm	640
GB 400-520 μm	550
GB 1000 μm	1070
GB 4000 μm	4250
EVA	3940

6.3.2.5. Characterization of the Coating

The coating structures were analyzed using a quantitative image analysis method described previously (161). The analysis comprised of the characterization of coating thickness distribution, the porosity, and the pore size distribution in the coating. The results were represented as the qualities critical to the coating functionalities, which are the minimum

coating thickness, the span of the coating distribution ($\frac{\Delta x_{90} - \Delta x_{10}}{\Delta x_{50}}$), the total porosity and the size of the largest pores ($d_{pore,90}$).

6.4. Results and Discussion

6.4.1. Prediction of Bed Relative Humidity

Different fluidized bed coating processes using various cores and process conditions were performed, resulting in different air temperatures at the outlet ($T_{a,out}$), which were measured and their data are given in Table 6-2. These data were split into two sets: one was used to obtain the heat loss coefficient and the other one was used to test the model.

The data from the first set, which are from the experiments #1 to 20, were fitted to Eq. 6-5. Using 'fminsearch' command in MATLAB®, different values of $C_{heatloss}$ were automatically tested into the model, until the differences between the calculated and the measured values of the air temperature at the outlet are minimized. The best value for $C_{heatloss}$ was found to be 6.1287$\pm$ 0.637x10^{-3} J/K.

Further, the model was validated using the air temperature at the outlet measured from experiments #21 to 42. These measured values were compared with the predicted air temperature at the outlet using the present heat and mass balance model (Eq. 6-5). The results shown in Figure 6-2 verify that our model predicts the air temperature at the outlet quite well, with a degree of fit of 0.99.

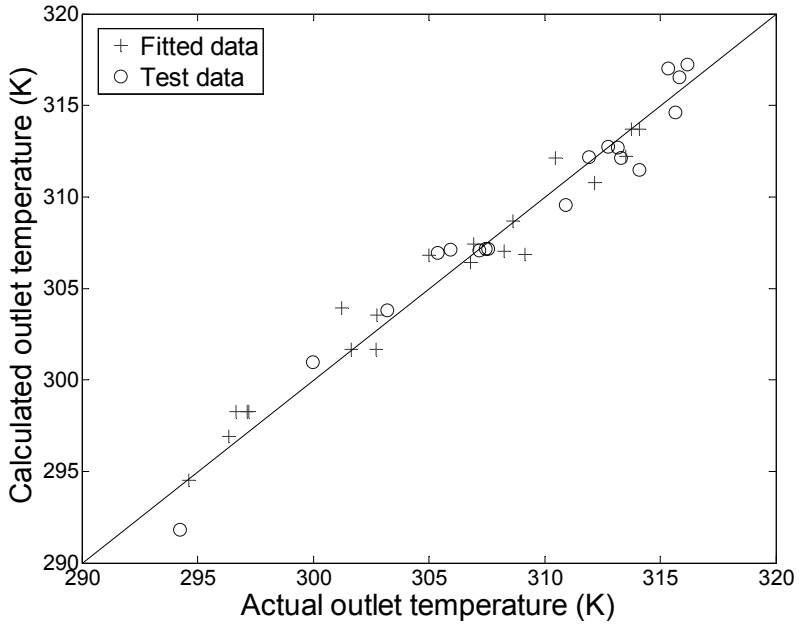

Figure 6-2. Verification of model to predict air temperature at outlet.

No significant effects were found of core properties (type and diameter) and droplet properties (atomization pressure) on the prediction quality of the model. The fact that the outlet air temperature can be well predicted by considering only the total fluidized bed system without looking at the core and droplet properties confirms the highly efficient energy transfer between the drying air and the coating solution assumed in the model.

Having determined the air temperature, the humidity of the air at the outlet enables the calculation of the bed relative humidity following the method described in the Appendix. The same value of RH_{bed} can be obtained from different combinations of spraying rate, inlet air temperature and flow rate. This suggests the suitability of using this process parameter to simplify the amount of process parameters to be evaluated for example during up-scaling.

6.4.2. Determination of Coating Process Regime

As discussed earlier in the theory section, the agglomeration tendency during the fluidized bed coating process is determined by the availability of liquid on the surface of the particle and the liquid strength to keep the particles together until solid bridges between the particles are formed. Intuitively, the amount of liquid on the particle surface can be minimized by fast drying or slow spraying. This condition is related to low bed relative humidity. Furthermore, spraying small droplets also enables fast drying, which will limit the number of successful particle coalescences. Therefore, both the bed relative humidity (RH_{bed}) and the relative (initial) droplet size to core size ($d_{droplet,o}/d_{core}$) were applied together with the excess of viscous Stokes number (ΔSt_v) criteria proposed by Ennis *et al.* (153) to develop a regime criteria in the fluidized bed coating process.

Amongst the experiments performed in this study, agglomeration occurred during experiments #1, 6, 11, 14, 27, 29, 31 and 32. In these experiments, more than 10% of the pellets were agglomerated. The bed collapsed after the process started in experiments #21, 24 and 39. These 11 experiments are classified to be in the agglomeration regime. The rest of the experiments were presumed to occur in the layering regime.

Figure 6-3 shows the ΔSt_v, RH_{bed} and $d_{droplet,o}/d_{core}$ conditions for each experiments, where the layering and agglomeration regimes were indicated in the figure labels. It is shown in this figure that the two regimes were separated by certain combinations of the ΔSt_v, RH_{bed} and $d_{droplet,o}/d_{core}$. The transition points were taken from the conditions which are in the middle of the conditions of experiments under layering condition which is close to the granulation

condition and vice versa. The corresponding the ΔSt_v, RH_{bed} and $d_{droplet,o}/d_{core}$ at the transition points were then fitted to the Partial Least Square (PLS) model resulting in Eq. 6-14 with degree of fit (R^2) of 0.95.

$$\Delta St_v = 1207 RH_{bed} + 301 \, d_{droplet} / d_{core} - 990 \tag{6-14}$$

This equation forms a surface plot that separates the layering and agglomeration regimes shown in Figure 6-3. This plot shows that a certain excess of viscous Stokes number is required to keep the process in the layering regime at a given bed relative humidity and relative droplet size. The inserted plot in Figure 6-3 is meant to illustrate better the correlation between these three variables. The color gradients in this image represent the different minimum values of the ΔSt_v required to be in a layering regime at various bed relative humidities and relative droplet size.

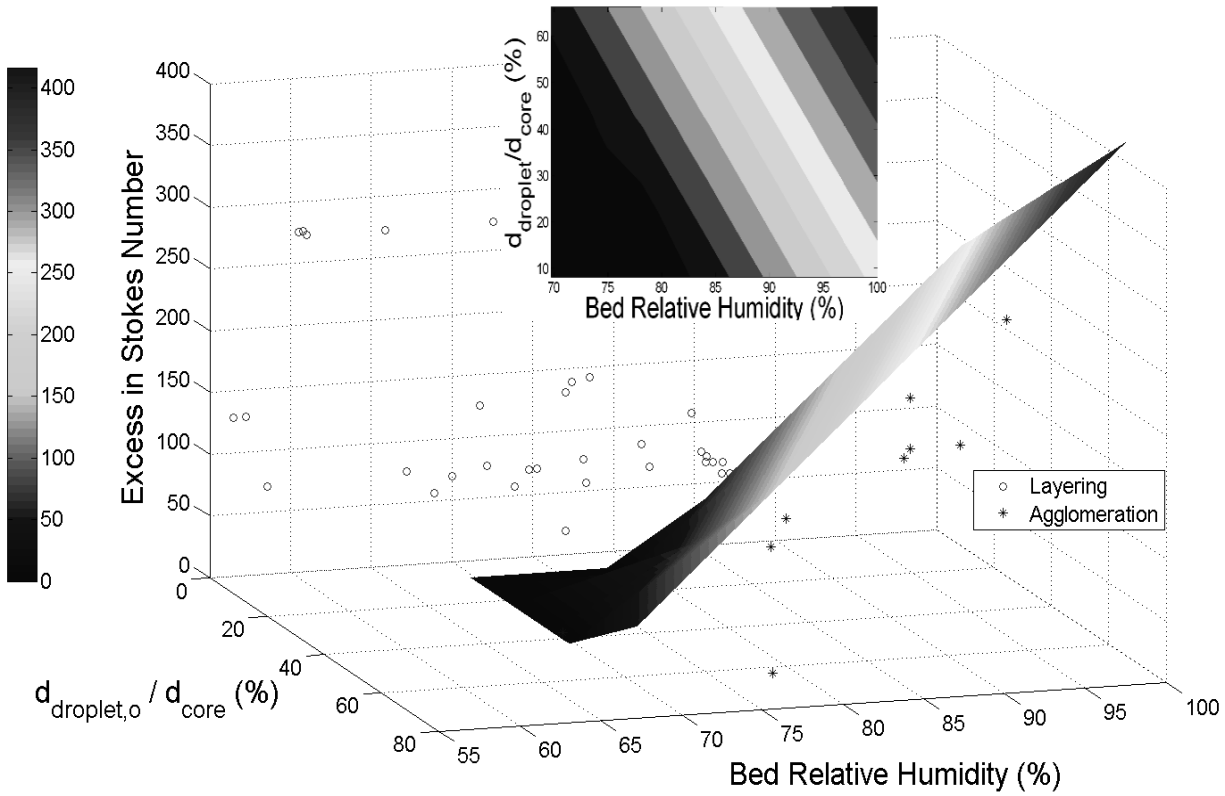

Figure 6-3. Process regime map determined by the combination of ΔSt_v, RH_{bed} and $d_{droplet}/d_{core}$ in the fluidized bed coater.

At a lower RH (*e.g.* at 70%), the ΔSt_v is shown to vary between 0 to about 40 (shown as dark and lighter blue colors, respectively) at a whole range of relative droplet sizes tested

(10-60%) (see the inserted plot in Figure 6-3). With increasing RH, the variation in ΔSt_v becomes bigger with increasing relative droplet size (*e.g.* varying from 250 to 400 when relative droplet size changes from 10 to 60% at 100% RH). The higher the bed relative humidity and the relative droplet size, the higher is the ΔSt_v required. Knowing the required ΔSt_v enables the process settings to be adjusted accordingly by changing *i.e.* the particle velocity, the particle size, the density and the viscosity of the coating solution. The ability to predict the occurrence of agglomeration helps to design the experimental program more effectively by selecting only those process settings that lead to the layering regime.

6.4.3. Process Adjustment and Its Effect on Coating Quality

Having determined the process windows for performing the coating process in the layering regime leads to the next step *i.e.* finding the optimum process conditions, which lead to the best coating quality. Coating quality can be described in terms of the uniformity of the coating thickness and the porosity of the coating. The uniformity of coating thickness can be quantified by the minimum coating thickness and the span of the coating thickness distribution. A very low minimum coating thickness is not desirable as it indicates the incomplete or poor coverage of the core particles. A wide span of the coating thickness distribution is either unwanted as it will lead to a big variation in the coating transport properties, which are particularly important for coating applied for controlled/extended release purposes.

The effects of the process conditions focusing on properties that describe the coating quality were further assessed. The shown results were taken from the experiments that used microcrystalline cellulose pellets (800-1000 μm) as core particles (of which conditions are listed in Table 6-2).

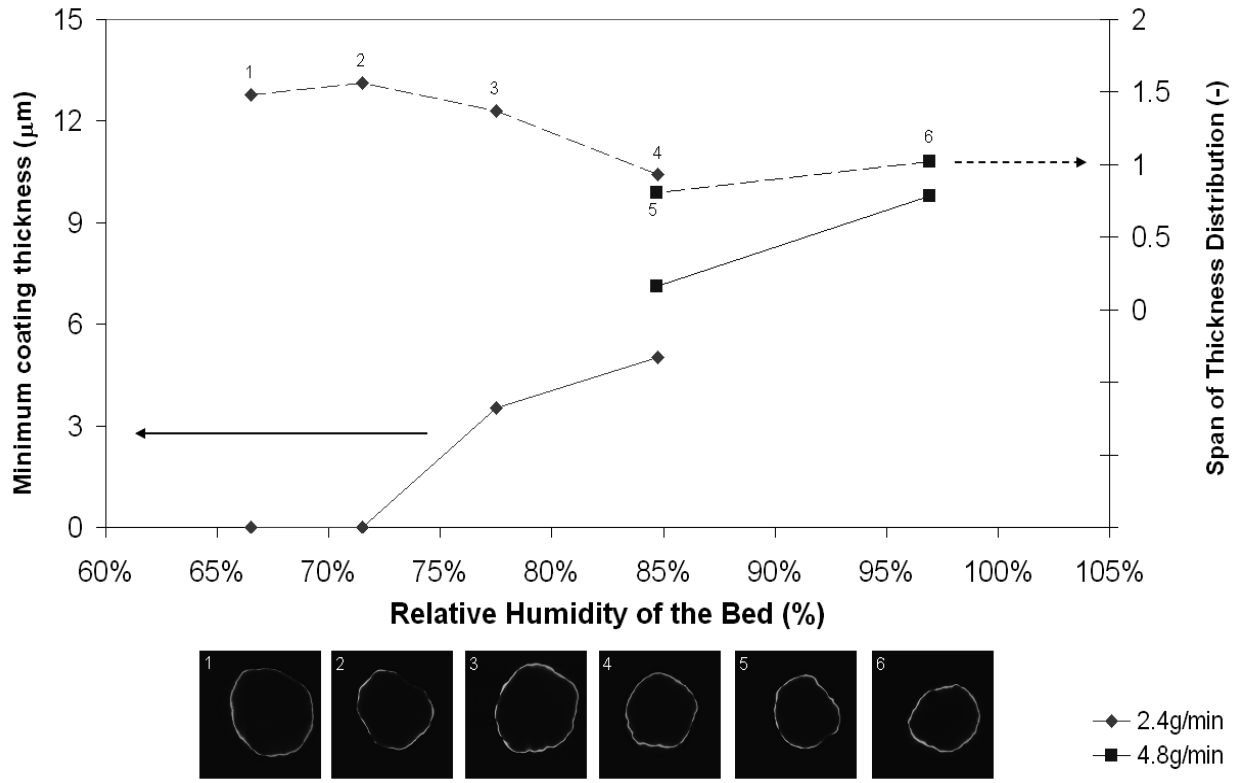

Figure 6-4. Effect of bed relative humidity on the minimum coating thickness and the span of the coating thickness distribution. *Underneath the plot* are the CSLM images of coated particles with corresponding numbering as the data plots.

Figure 6-4 shows the effect of increasing the bed relative humidity (in this case by reducing the inlet air temperature) on the coating thickness distribution. It is shown that a maximum in the minimum coating thickness and a minimum span of coating thickness distribution were achieved when the coating process was performed at a high relative humidity of the bed.

Figure 6-5 shows another positive effect of increasing the bed relative humidity on coating quality, *i.e.* reduction of the coating porosity and the pore size. At high relative humidity, there is less chance for premature drying of the coating droplets. Consequently, the coating droplets are still wet upon collision with particles enabling the droplet to spread well on the particles, which results in a more homogeneous and less-porous coating structure.

A discontinuity in the correlation between the bed relative humidity and the coating quality is noticed in Figure 6-4 and Figure 6-5 between processes performed using spraying rates of 2.4 and 4.8 g/min. At these different spraying rates, both the relative initial droplet size and the spraying flux rate (defined as the fractional area of particles sprayed per unit of time) are changed.

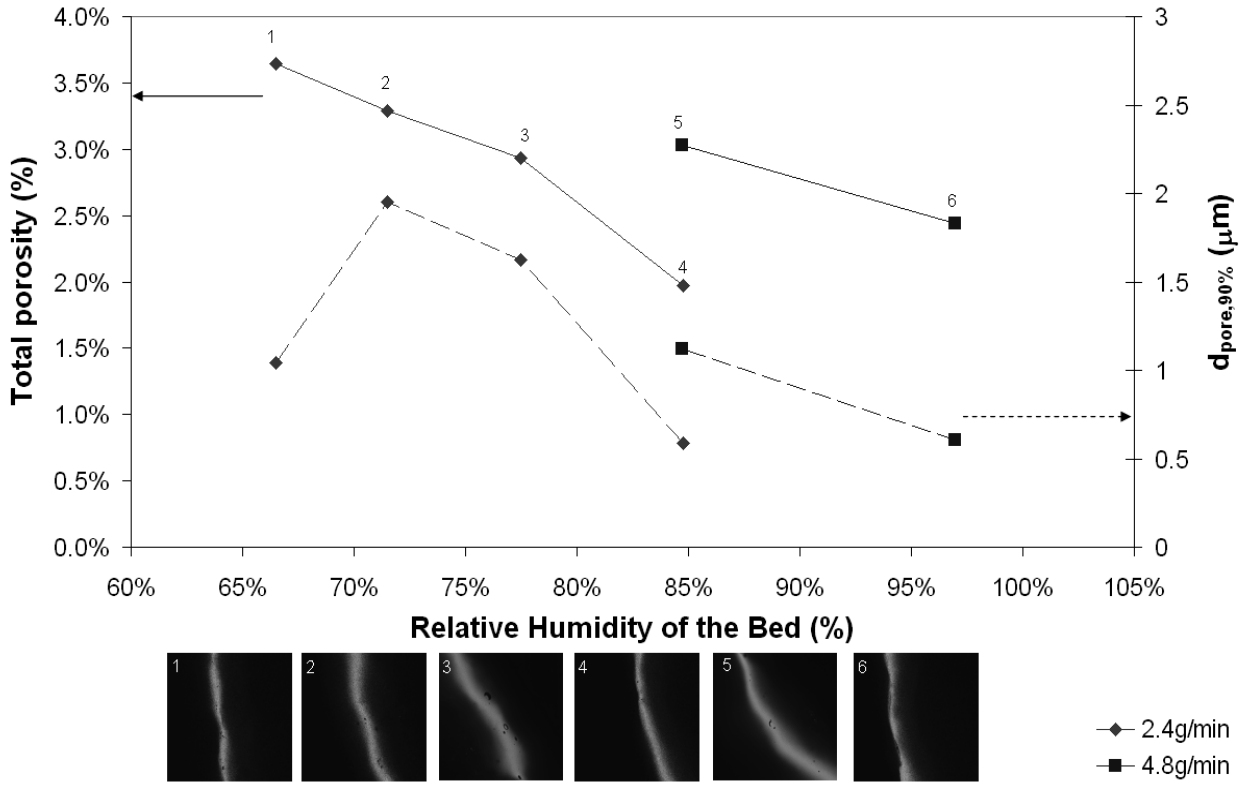

Figure 6-5. Effect of bed relative humidity on coating porosity and pore size. *Underneath the plot* are the CSLM images of coating layer on particles with corresponding numbering as the data plots.

The inter-dependency between process parameters in the fluidized bed coating process has been identified. The inlet air temperature and the spraying rate together influence the relative humidity. Either the changes in the atomization pressure or in the spraying rate vary the (relative) initial droplet size. Together with the spraying rate, the respective droplet size will determine spraying flux rate. Consequently, it was difficult to vary one condition without changing other conditions and keeping the process in the layering regime at the same time.

Figure 6-6 illustrates the inter-relationship between these process settings and the range of the process parameters varied in this study, which is limited to the process settings that avoid the occurrence of agglomeration. This figure shows for example that the bed relative humidity can be varied extensively without causing any agglomeration and any significant changes in the spraying flux rate when the droplets sprayed are small enough. Moreover, this figure supports the discussion on the selection of the process settings for achieving the best coating quality based on Figure 6-7 and Figure 6-8.

Figure 6-7 and Figure 6-8 were plotted to illustrate the combined effect of these process conditions on minimum coating thickness and coating porosity, respectively. These plots were made by making a data grid from the experimental data using a "v4" method in MATLAB®.

High coating quality implies the absence of uncoated areas/ areas with a very thin layer, meaning that the minimum coating thickness is close to the average thickness. The average coating thickness obtained in this study is between 25-30 μm. Figure 6-7 shows that the minimum of coating thickness is closest to the average thickness at bed relative humidity close to saturation and at droplet size around 10 to 30% of particle size, which corresponds to high spraying flux rate (~7-10x10^{-3} s^{-1}). A high spraying flux rate implies to a high probability for droplets to cover the particle surface. The relative droplet size indicates the fraction of particle covered by a droplet every time it reaches the particle. The actual coverage of particle by droplets can therefore be estimated from the product between the probability (the spraying flux rate) and the droplet size relative to the particle size. When these factors are higher, the coating coverage on the core particles becomes better. This explains why at low relative droplet size (below 5%), the minimum coating thickness is low, although the spraying flux rate is high. A similar reason exists for the coating process using high relative droplet size (above 30%), where the spraying flux rate is low and therefore the minimum coating thickness obtained is low.

Figure 6-8 shows similar effects of the combination between the relative humidity, the relative droplet size and the spraying flux rate on the coating porosity. Minimum coating porosity is desired. This can be obtained by performing the coating process at a bed relative humidity close to saturation. At this point, the variations in the relative droplet size as well as in the spraying flux rate do not influence the coating porosity. Close to saturation, droplets evaporate slowly, which facilitates enough time for the coating solution to rewet the precursor film and fill in the existing pores leading to a dense coating. Porous coating is obtained at low bed relative humidity at high relative droplet size. This condition corresponds to a low spraying flux rate. This result shows the severe impact of the combination between fast drying and low distribution of droplets on the coating porosity obtained.

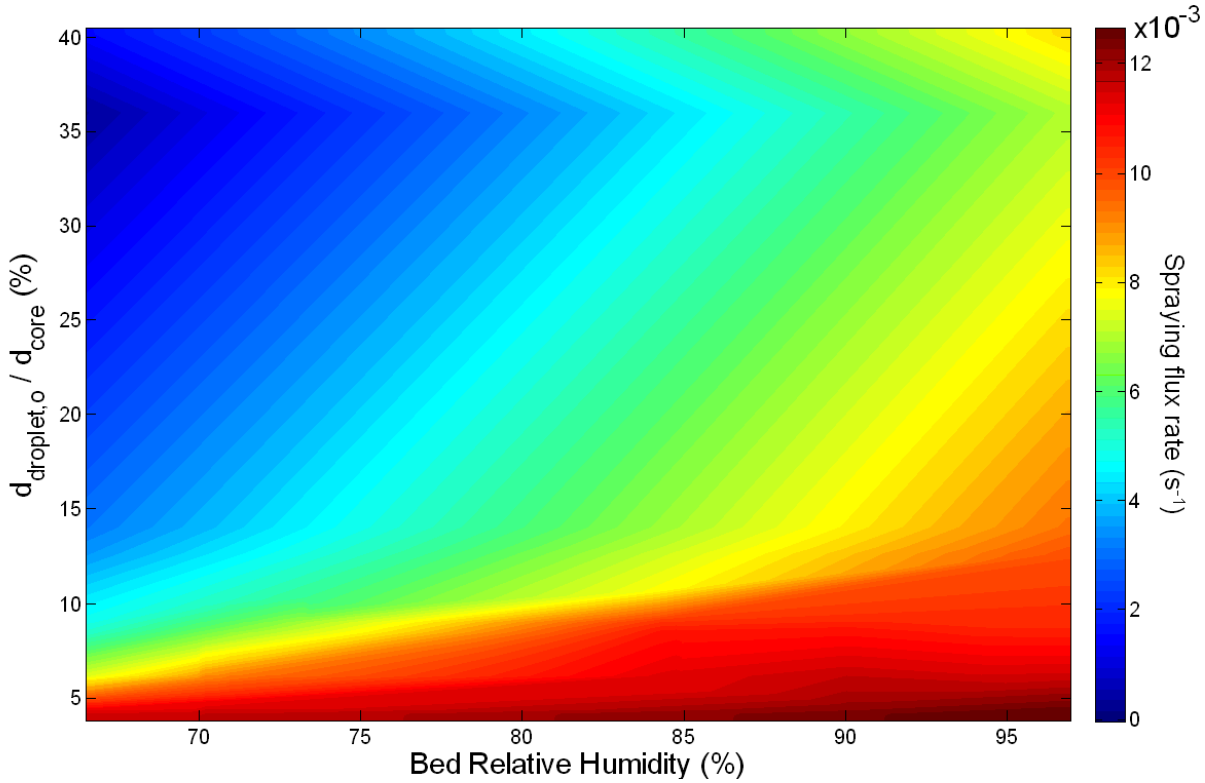

Figure 6-6. The combination of process settings used in this study between the relative droplet size, bed relative humidity and spraying flux rate (defined as the fractional area of particle sprayed per unit time)

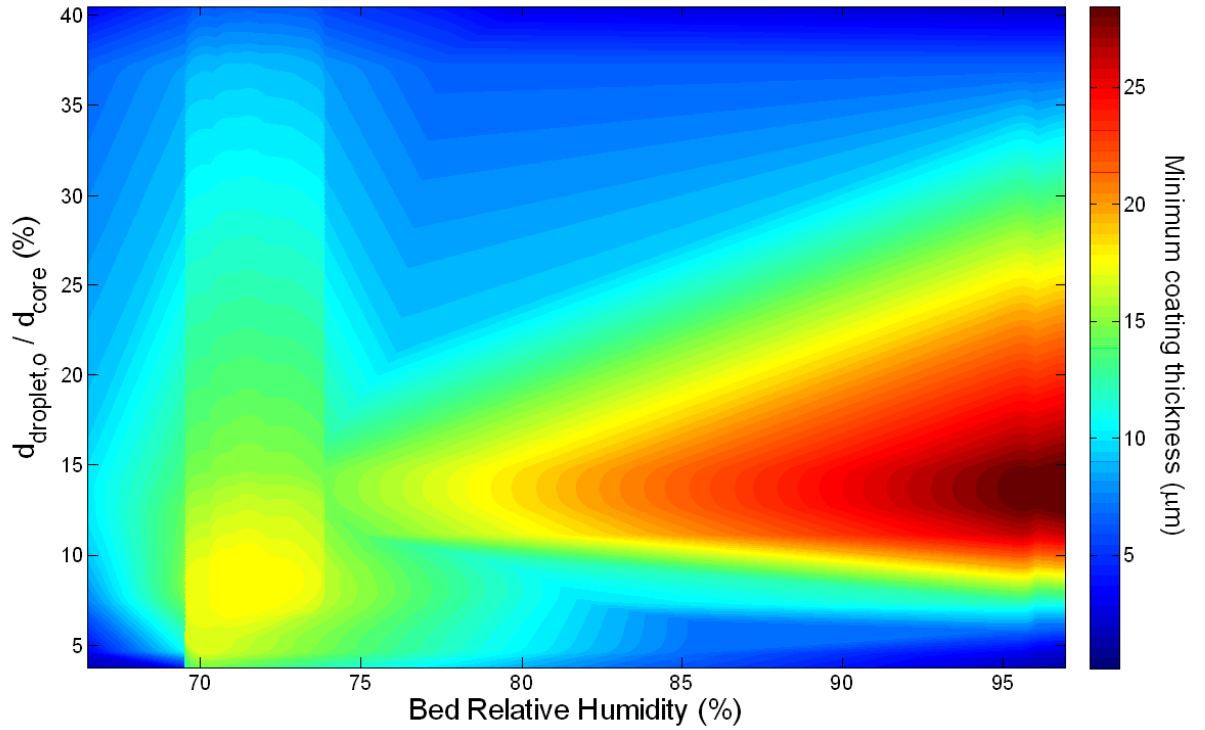

Figure 6-7. A contour plot of the effect of the relative initial droplet size and the bed relative humidity on the minimum coating thickness.

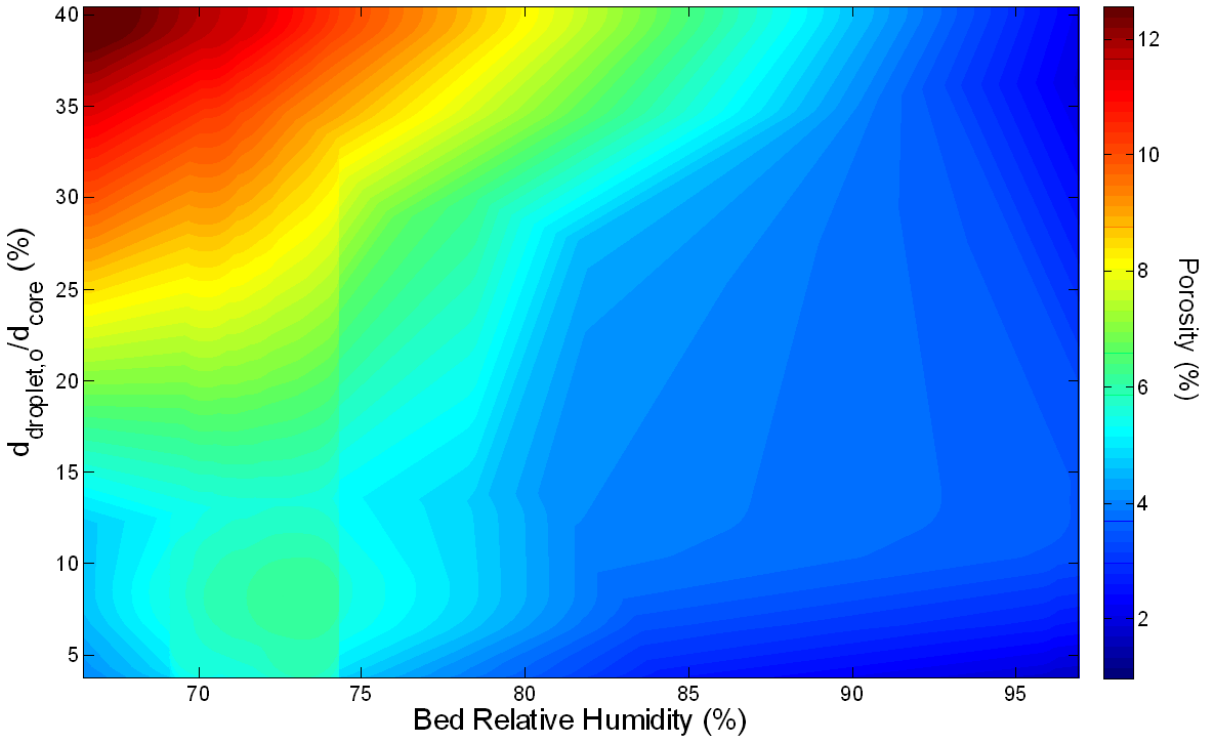

Figure 6-8. A contour plot of the effect of the relative initial droplet size and the bed relative humidity on the coating porosity.

6.5. Conclusions

In this study, the relationship between the excess in viscous Stokes number and the bed relative humidity and the relative droplet size has been developed. These criteria have been used to determine the process regime inside a fluidized bed coater that lead to the best quality of the coating.

The inter-dependency between the bed relative humidity, the droplet size and the spraying flux rate (fractional area of particle sprayed per unit of time) has been identified. They were shown to be important in controlling the coating quality, which influences have to be assessed at once. High coating quality defined as having uniform coating thickness (minimum coating thickness close to mean coating thickness) and low porosity can be achieved by performing the coating process close to saturation. Using a small droplet size leads to a high spraying rate that is required for obtaining high coating quality. Nevertheless, the droplet size should not be too low, since that may cause incomplete coverage of the core particles.

ACKNOWLEDGEMENTS

The authors would like to thank Mario Campana for his contribution on the derivation of the correlations for the hydrodynamic properties of the fluidized bed coater used for our study. We would also like to thank Friesland Food Research Centre Deventer, The Netherlands, especially Drs. Marcel Paques for letting us use their CSLM facility and Ing. Anno Koning for performing the CLSM measurements.

APPENDIX

The drying path by air inside a fluidized bed coating process is schematically given in Figure 6-9. In this figure, the adiabatic saturation line is represented by a blue solid line. When there is heat loss, the drying process in the fluidized bed coater no longer follows the adiabatic saturation line but a path, which typically follows the non-adiabatic line as given in this figure. Under this condition, the maximum amount of water vapor that the drying air can contain before it becomes saturated (saturated humidity of air, $Y_{a,sat-nonad}$) is lower than that in the adiabatic process ($Y_{a,sat-ad}$).

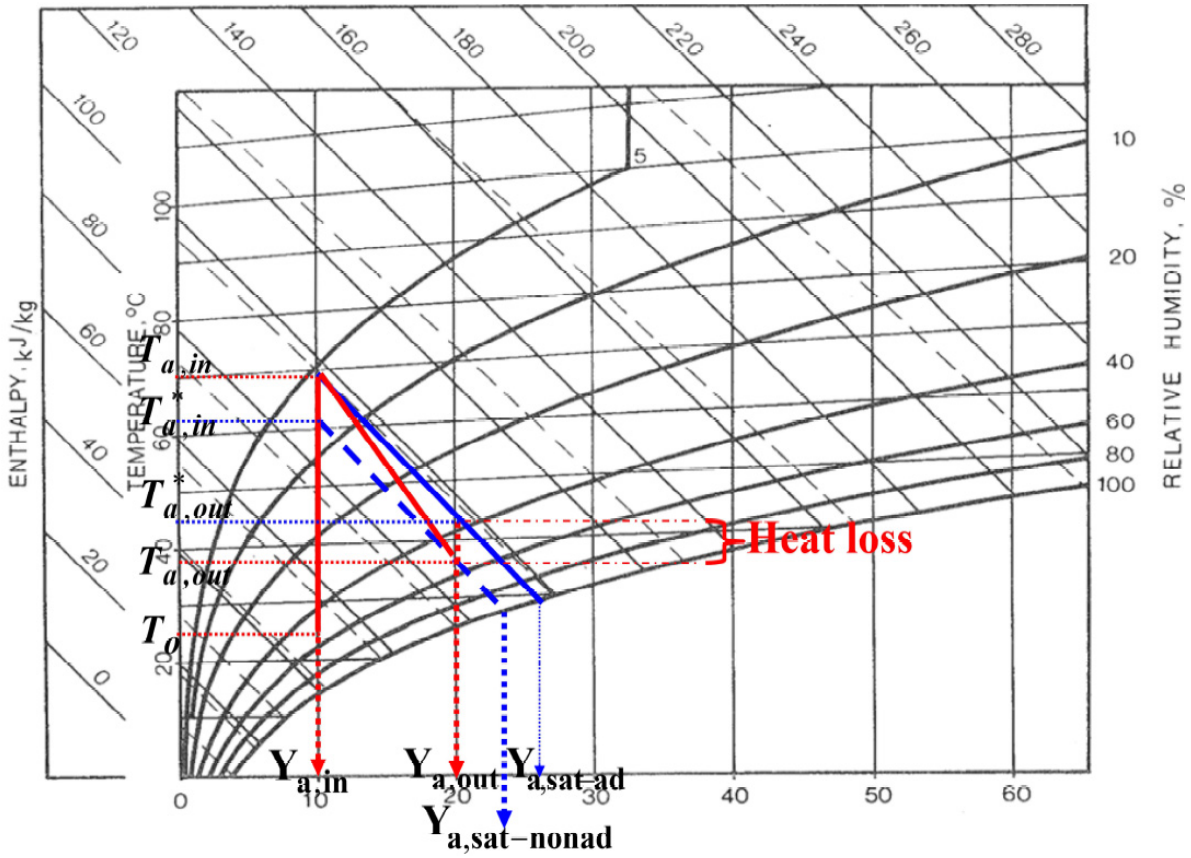

Figure 6-9. Schematic diagram of enthalpy, temperature and humidity changes during fluidized bed coating process. Blue solid line represents the adiabatic saturation process, while red line represents the non-adiabatic drying path in the actual process.

In this study, the $Y_{a,sat-nonad}$ was estimated using a hypothetical adiabatic saturation line. Due to heat loss, the air temperature at the outlet ($T_{a,out}$) is also lower than that in the adiabatic process ($T^*_{a,out}$). A hypothetical adiabatic saturation line was drawn, which passes the actual air temperature at the outlet ($T_{a,out}$), shown as a blue dash line in Figure 6-9. This line starts at an inlet air temperature ($T^*_{a,in}$) lower than the actual inlet air temperature ($T_{a,in}$).

Working in the same range of air humidities at the inlet and the outlet in both adiabatic and non-adiabatic processes, the difference between the $T_{a,in}$ and the $T^*_{a,in}$ is equal to the difference between the outlet air temperature in adiabatic ($T^*_{a,out}$) and non-adiabatic ($T_{a,out}$) conditions, as depicted in Eq. 6A-1. The $T^*_{a,out}$ was calculated using Eq. 6-5 by neglecting the term $C_{heatloss}$.

$$T^*_{a,in} = T_{a,in} - \left(T^*_{a,out} - T_{a,out}\right) \tag{6A-1}$$

Graphically, the actual saturated humidity of air ($Y_{a,sat-nonad}$) could be determined by following the hypothetical adiabatic saturation line using a psychrometry chart. To enable automatic calculations using a computer, in this study, it was calculated using the following equations:

- Eq. 6A-2 describes the correlation between the saturation water vapor pressure and temperature, which is valid for the temperature range between 25 and 100°C (125).
- Substituting this relation, to Eq. 6A-3, the air temperature at saturation point could be calculated. For water-air mixture, $\frac{c_s}{\lambda}$ is equal to 4.45x10^{-4} (125).
- Further on, the saturated humidity of air ($Y_{a,sat-nonad}$) was calculated using Eq. 6A-4. Finally, the bed relative humidity (RH_{bed}) was calculated using Eq. 6A-5.

$$P_{sat} = 2.740938\text{x}10^{-37}\left(T_{a,sat}\right)^{16.19334} \tag{6A-2}$$

$$T_{a,sat} = T^*_{a,in} + \frac{Y_{a,in} - \frac{P_{sat}}{P - P_{sat}} \times \frac{Mw_w}{Mw_a}}{c_s / \lambda} \tag{6A-3}$$

$$Y_{a,sat-nonad} = \frac{P_{sat}}{P - P_{sat}} \times \frac{Mw_w}{Mw_a} \tag{6A-4}$$

$$RH_{bed} = \frac{Y_{a,out}}{Y_{a,sat,non-ad}} \times \frac{Mw_w / Mw_a + Y_{a,sat,non-ad}}{Mw_w / Mw_a + Y_{a,out}} \tag{6A-5}$$

NOTATIONS

Cp	Specific heat capacity of dry air [=] kJ/kg.K
C_s	Humid heat [=] J/g.K
Cv	Specific heat capacity of water vapor [=] kJ/kg.K
D	Mean diameter [=] m
$\dot{F}$	Mass flow rate [=] g/s
$d_{pore,90}$	Maximum diameter of 90% number fraction of pores in a coating [=] μm
H	Thickness of the liquid surface layer [=]
h_a	Characteristic height of surface asperities [=] m
h_d	Droplet height [=] m
K	Ratio of specific heats, Cp/Cv [=] -
Mw	Relative molecular weight [=] g/mol
P	Partial pressure [=] Pa
P_{tot}	Atmospheric pressure [=] Pa
Q	Volumetric flow rate [=] m^3/s
R	Universal gas constant [=] J/mol K
Re	Reynold's number [=] -
RH	Relative humidity [=] %
St_v	Viscous Stokes number [=] -
St_v^*	Critical Stokes number [=] -
T	Temperature [=] K
U	Velocity [=] m/s
V	Volume [=] m^3
We	Weber number [=] -
X	Mass fraction [=] -
Y	Humidity [=] -
ΔSt_v	Excess in the viscous Stokes number (St_v-St_v^*) [=] -
λ	Specific enthalpy of evaporation [=] J/g
γ	Surface tension of coating solution [=] N/m
μ	Viscosity of coating solution [=] Pa s
ρ	Density [=] g/m^3
θ	Contact angle of coating solution [=] °

Subscripts

A	Air
Ad	Adiabatic condition
Atm	Atomization
Bed	Particle bed
D	Droplet
d,o	Droplet at initial condition
In	At the inlet of the fluidized bed equipment
N	Nozzle/atomization
Nonad	Non-adiabatic condition
Orifice	Through the orifice of nozzle
Out	At the outlet of the fluidized bed equipment
P	Particle/Pellets/Granules
S	Solution
Sat	At saturation
Tip	At the tip of the nozzle
V	Water vapor
W	Water